Available online at www.sciencedirect.com
SCIENCE DIRECT®
Journal of Solid State Chemistry 177 (2004) 3650–3659
JOURNAL OF SOLID STATE CHEMISTRY
http://elsevier.com/locate/jssc

Preparation and electrorheological characteristic of Y-doped $BaTiO_3$ suspension under dc electric field

Jian-Bo Yin and Xiao-Peng Zhao*

Institute of Electrorheological Technology, Department of Applied Physics, Northwestern Polytechnical University, Xi'an 710072, China

Received 14 April 2004; received in revised form 28 May 2004; accepted 6 June 2004

Available online 19 August 2004

Abstract

The electrorheological (ER) effects of $BaTiO_3$ or other perovskite materials with high dielectric constant are presumed to be large. However, their weak ER activity is very puzzling. In this study, we choose cubic $BaTiO_3$ and first achieve its ER enhancement under dc electric field by modifying its intrinsic structure with doping rare earth Y ions, which are synthesized by means of sol–gel technique. DSC-TG, FT-IR, XRD, ICP and XPS techniques are used to characterize thermal, structure and component change of materials. It is demonstrated that Y^{3+} substitutes for Ba^{2+}, which causes lattice-distorting defects. Rheological experiments show that Y-doped $BaTiO_3$ suspension has notable ER effect and clear fibrillation structure under dc electric field, while the pure cubic $BaTiO_3$ suspension suffers from electrophoretic effects and its ER effect is very weak. The ER effect of typical Y-doped $BaTiO_3$ ER suspension is ten times that of pure $BaTiO_3$ ER suspension. Based on the electrical measurements, the enhancement of ER activity of $BaTiO_3$ may be attributed to the increase of conductivity due to Y-doping. The enhancement in ER activity of cubic $BaTiO_3$ under dc electric field by doping rare earth Y ions is helpful to further understand the perovskite-based ER materials with high dielectric constant but low ER activity.

Keywords: Rare earth; $BaTiO_3$; Cubic; Doping; ER effect

1. Introduction

Electrorheological (ER) fluid usually consists of microscopic dielectric particles in insulating liquid. Under an applied electric field, the dispersed dielectric particles will be polarized and attracted to each other to form chain or column structures. These chains and columns enable ER fluid to suddenly increase its viscosity and even change from a liquid-like state to a solid-like state that has a yield stress to resist shearing deformation. Interestingly, the viscosity change or liquid–solid state transition of ER fluid is reversible as soon as the applied electric field is removed [1–3]. Because of the reversible and quick response to external electric field, ER fluid has attracted much interest in uses in various mechanical devices such as clutches, valves, damping devices, and other areas such as polishing, display, ink jet printer, human muscle stimulator, mechanical sensor, and preparation of photonic materials or devices [4–8]. In order to meet the requirements of most of these applications, it is necessary for ER fluid to have high-yield stress. Currently, researchers mainly focus on two ways to enhance the strength of an ER fluid. One is to change the measurement model or condition on the basis of the effect of microstructure inside the column of ER fluid on yield stress [9–11]. The other is to design and prepare high-performance ER materials. The material systems including semiconductive polymer [12,13], aluminosilicate [14], polymer ion conductor [15], carbonaceous [16], core/shell composite particles [17,18], and nanocomposite [19–23] have been employed to obtain active ER materials. Although these materials open novel ways to prepare ER materials, the experimental results are still far from the original assumption and the present ER materials are still limited in applications because of either low-yield stress, temperature instability, or sedimentation.

*Corresponding author. Fax: +86-29-8849-1000.
E-mail address: xpzhao@nwpu.edu.cn (X.-P. Zhao).

0022-4596/$ - see front matter © 2004 Elsevier Inc. All rights reserved.
doi:10.1016/j.jssc.2004.06.013

Because of the high dielectric constant, the use of perovskite materials such as $BaTiO_3$, $SrTiO_3$ and $CaTiO_3$ as ER active substrates have been the focus of attention for some time [24–35]. In terms of dielectric polarization mechanisms, the ER effect of perovskite materials is presumed to be large because of the high dielectric constant. However, some investigations showed that pure dry perovskite materials were fairly weak in ER effect; even $BaTiO_3$ was suffered from electrophoretic effects under high dc electric field [24,25,27,28]. This was amazing and could not be understood by conventional polarization mechanisms. More studies had been carried out in order to understand the reasons of weak ER effect of perovskite materials. Low conductivity or dielectric loss, originating from intrinsic fast polarization process of perovskite materials under dc or low frequency ac electric field, had been suggested to be responsible for the poor ER effect under dc or low frequency ac field [33–38]. It had been reported that perovskite materials, in particular $BaTiO_3$, as substrate were frequency-promoted, which was explained according to the mechanism of dielectric constant and conductivity mismatch [28,32]. In order to overcome the poor ER effect and well understand ER mechanism, some researchers obtained ER enhancement by means of adsorbing water or surfactant onto the surface of $BaTiO_3$ particles to modify its polarization and conduction properties [26,30,38]. But it should be noted that the extrinsic effect of adsorbed water or surfactant is not helpful in understanding the intrinsic properties of $BaTiO_3$ or other perovskite materials that result in the weak ER effect. Furthermore, to our knowledge, no high-performance perovskite-based ER materials have been produced. Thus, it is of great interest to design and prepare perovskite-based ER materials in order to consider the ER mechanisms and explore new ways to prepare high-performance perovskite-based ER materials.

It is widely accepted that the ER effect originates from the dielectric polarization of particles dispersed in oil phase. Not only large polarization ability relating to dielectric constant but also good polarization response and stability relating to suitable conductivity (10^{-8}–10^{-7} S/m) or dielectric loss tangent ($\geqslant 0.1$) mainly dominate high ER effect [1,12,29,37,39,40]. It is well known that the chemical natures including molecular or crystal structure, composition and microstrucutre of materials are important to the dielectric and conduction properties. Thus, it is possible to modify the dielectric and conduction properties for ER enhancement by adjusting the crystal structure, composition and microstrucutre of ER materials. Based on this idea, we found that the weak ER activity of TiO_2, which also had high dielectric constant but low ER activity, mainly originated from its low active natural structure that could not supply optimal dielectric and conduction properties for high ER activity. Then we first demonstrated that the ER activity of TiO_2 could be improved by modifying its dielectric and conduction properties, which was achieved by adjusting its internal structure or microstructure in the previous studies [41–45]. In this study, we first achieve ER enhancement of $BaTiO_3$ by choosing $BaTiO_3$ with a cubic crystal phase as substrate and modify its intrinsic structure by doping rare earth ions method. The rheological properties are studied as a function of electric field strength, doping degree and shear rate. Based on the investigation about chain structure and electrical properties of ER suspensions, we preliminarily discuss the effect of rare earth Y-doping on ER behaviors of $BaTiO_3$.

2. Experimental

2.1. Materials synthesis

Particles of cubic pure and Y-doped $BaTiO_3$ with different doping degrees (the doping degree or Y content x is defined by $Ba_{1-x}Y_xTiO_3$) were obtained from barium acetate (Tianjin reagent Co., China), yttrium acetate (Tianjin reagent Co., China), titanium tetrabutoxide (Shanghai JinShan reagent Co., China) and distilled water by the modified sol–gel technique [46]. All chemical reagents were used as received without further purification. In order to avoid the phase separation of inorganic salt from the solution and increase the doping degree, we specially chose water-free alcohol and acetate acid (v/v = 1/1) as a mixed solvent. The H_2O/Ti mole ratio was 1.0–1.5 and Ti concentration was 0.5–0.8 mol/L in the resulting solutions. The resulting clear solutions were aged in the sealed container at ambient temperature for two weeks to slowly form very transparent gels. The gels were then dried carefully in a vacuum at ambient temperature, and the dry gels were milled with mortar and subjected to the following stepwise calcination programs in air in a furnace: 2 h at 200°C, 2 h at 400°C, 2 h at 600°C and 4 h at 800°C. Then, the cubic $BaTiO_3$ and doped $BaTiO_3$ particles were produced.

2.2. Characterization

To determine the thermal character and change of chemical structure of xerogel during calcination process, DSC-TG (SH-500, NET2SCH-Gerateban Gabh Thermal Analysis) and Infrared spectra (EQUIOX55 Fourier Transform Infrared Spectrometer) were employed. The crystal structure of samples was determined by X-ray powder diffraction (XRD) patterns that were carried out on a D/MAX-IIIC X-ray diffractometer with Cu$K\alpha$ irradiation at 40 kV/40 mA. Lattice parameters were calculated using data obtained from a diffractometer,

which was calibrated with an external Si standard. X-ray photoelectron spectroscopy (XPS) measurements were done with a PHI Quantum 2000 XPS System with a monochromatic Mg$K\alpha$ source and a charge neutralizer. All the binding energies were referenced to C 1s peak at 284.6 eV of the surface adventitious carbon. IRIS Inductively Coupled Plasma (ICP) was used to measure the element concentration.

2.3. Preparation of ER suspension

First, to produce ER suspensions, the pure and doped $BaTiO_3$ particles (All the produced particles were 0.5–5.0 μm in size, with polydisperse estimated by JSM-5800 scanning electron microscopy and density determined by using a pycnometer was 4.74–5.02 g/cm^3) were fully dehydrated in a vacuum at 150°C for 8 h in order to remove any physiadsorbed water. Second, the dried particles were mixed quickly with dimethyl-silicone oil ($\varepsilon_f = 2.60-2.80$, $\rho_f \approx 0.997$ g/cm^3 and $\eta = 50$ mP as at 25°C, Shin-Etsu Silicone Co, Japan) in a particle volume fraction of 18% (the volume fraction ϕ is defined by a volume percentage of particle relative to the total suspension volume, i.e., $\phi = V_p/(V_p + V_f)$, where V_p is the volume of particles and V_f is the volume of silicone oil). No additives were added in suspensions. Finally, the suspensions were specially milled for 0.5 h in a carnelian mortar for well-mixing particles with silicone oil.

2.4. Electrorheological measurements

The basic structure of pure $BaTiO_3$ and doped $BaTiO_3$ ER suspensions without electric field and with electric field was observed by a high-definition Nikon ALPHAPHOT-2 optical microscopy. Rheological experiments were performed by using an NXS-11 coaxial cylinder rotational rheometer with a Coutte geometry system whose maximum measurable stresses was 2.760 kPa, and a WYZ-010 dc high-voltage generator. The gap of Coutte systems was 2.0 mm. The maximum current density through viscometer was limited to 0.5 mA/cm^2. The maximum voltage of dc high-voltage generator was 10 kV and the current was limited to 2.0 mA. The suspensions were placed into the gap between the stationary cup and the rotating bob. Before reading stresses, we had initially applied the electric field on suspensions for 0.5 min and then sheared. The shear stress was measured as a function of shear rate that was varied from 2.110 to 136.5 s^{-1}. The electric field-enhanced shear stress, $\Delta\tau$, was defined by the relation $\Delta\tau = \tau_E - \tau_0$, where τ_E is the shear stress at a shear rate $\dot{\gamma} = 10.51$ s^{-1} under electric field and τ_0 is the shear stress at a shear rate $\dot{\gamma} = 10.51$ s^{-1} under zero electric field [29].

2.5. Dielectric and conduction measurements

Owing to the difficulty of directly measuring the dielectric and conductivity properties of particles, we used flakes, which were prepared by pressing the powders to 40 MPa in a 5 mm stainless steel die, to measure their dielectric constant and conductivity. Electrodes were fabricated from Ag paste and then fired to 800°C to remove organics. The flakes were fully dried in 150°C and placed in a vacuum glass tube in order to avoid the influence of moisture. The capacitance C was directly measured by an automatic LCR meter (WK-4225, Germany) at the frequency of 10^3 Hz with an applied bias voltage of 2 V. The dielectric constant ε was derived from the measured C according to the conventional relation, $\varepsilon = Cd/(\varepsilon_0 S)$, where ε_0 is the dielectric constant of vacuum, i.e. 8.85×10^{-12} F m^{-1}, and d is the thickness of pellets between electrodes and S is the contact area of electrodes. Conventional dc conductivity, σ_{dc}, of ER materials was derived from the leaking current density through pellets according to Ref. [13], j, with a microdetector in a high dc electric field, E_0, of 2, 3, 4, 5, and 6 kV/mm according to the relation, $\sigma_{dc} = j/E_0$.

3. Results and discussion

3.1. Characterization

Figs. 1 and 2 show the DSC-TG pattern of Y-doped $BaTiO_3$ xerogel and corresponding XRD patterns at different calcination temperature. The endothermic effect at 78.1°C and the sample weight loss represent the loss of residual water and solvent. The exothermic peaks at 315°C and 410°C are attributed to the combustion of a residual alkyl group. After 400°C, the sample still has an amorphous structure. According to the XRD peak of the sample, around 23° originating from carbonate phase at 600°C, we conclude that the exothermic peaks at 553°C and 590°C may be mainly due to the formation of barium or yttrium carbonate when barium or yttrium salt is partly carbonized. However, as shown by the exothermic peak at 741.5°C and continuous weight loss and XRD pattern after 800°C, the carbonate disappears with increasing temperature, and in the meantime the well-crystallized $BaTiO_3$ phase is formed. After 800°C, no further weight loss is detected.

Fig. 3a shows the typical FT-IR spectra of doped $BaTiO_3$ xerogel before calcination. The –OH-stretching adsorption band at 3420 cm^{-1} and special adsorption bands of Ba(Y)-$COOHCH_3$ at 1560 and 1418 cm^{-1} have been noted in spectra. Fig. 3b and b′ show the FT-IR spectra of pure $BaTiO_3$ and doped $BaTiO_3$ after calcination of 800°C. Only the double peaks between

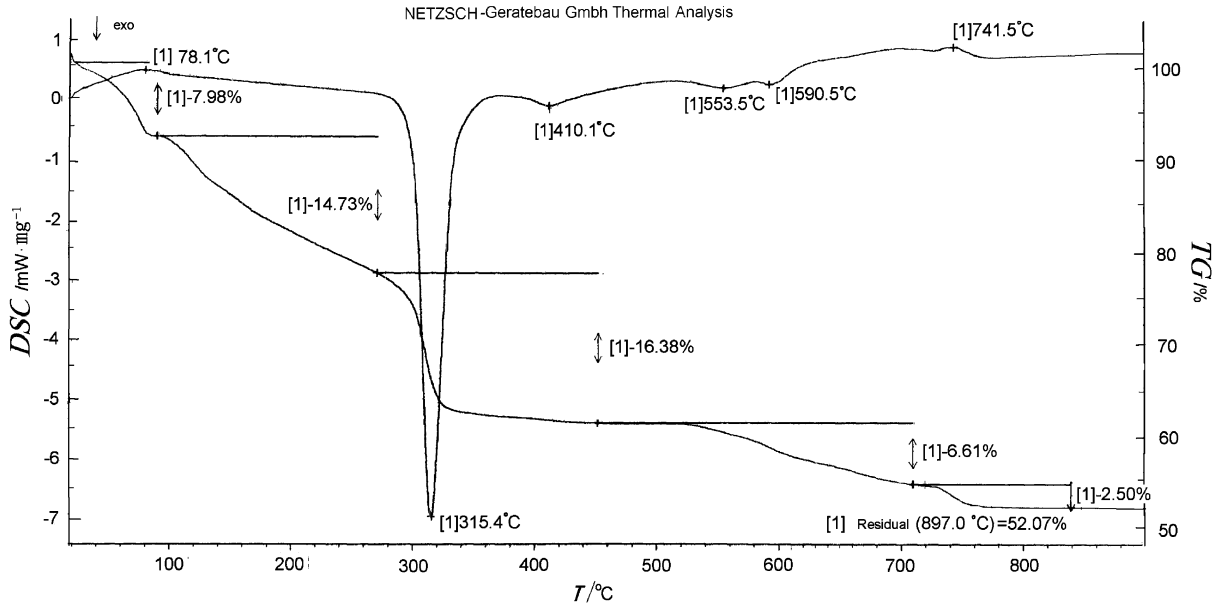

Fig. 1. DSC-TG curve of 13.8 mol% Y-doped $BaTiO_3$ xerogel powders.

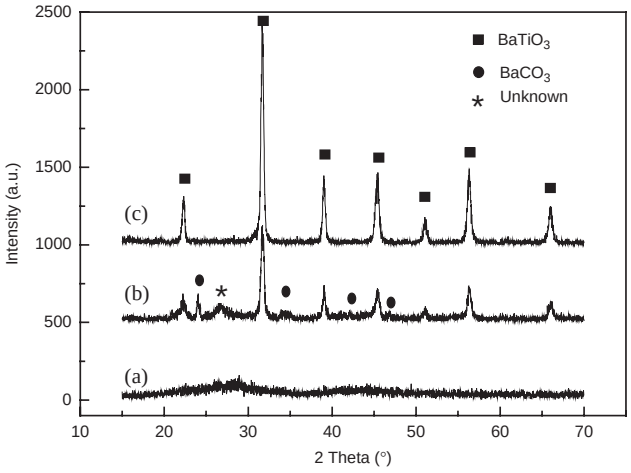

Fig. 2. XRD patterns of Y-doped $BaTiO_3$ powder at different calcined temperatures: (a) 400°C, (b) 600°C, and (c) 800°C.

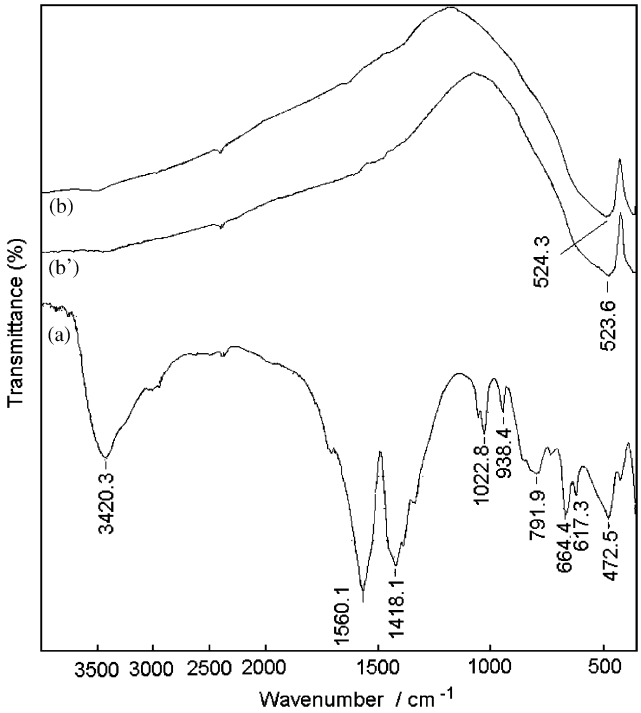

Fig. 3. FT-IR spectra of Y-doped $BaTiO_3$ samples: (a) before calcinations, and (b) after calcinations at 800°C (b′ is FT-IR spectra of pure $BaTiO_3$ after calcinations at 800°C).

526 and 400 cm^{-1}, which represents the typical M–O adsorption bands in $BaTiO_3$ crystal, can be observed. No peaks originating from organic compounds are found, which indicates all organic compounds have been well removed by calcination.

According to previous reports [47,48], the Y incorporation in $BaTiO_3$ was complex and solid solution limit was relatively low. In order to understand the concentration of components and Y incorporation in samples, inductively coupled plasma (ICP) and XRD techniques were used to quantitatively measure the element concentration and crystal structure change, respectively. According to ICP measurements, the mole ratio of Ba/Ti is 0.999/1 for pure $BaTiO_3$. The mole ratio of Y element is in accordance with the designed concentration. For example, the mole ratio of Y 8.9 mol% in designed 9 mol% doped sample and 13.8% in designed 14 mol% doped sample. Fig. 4 shows the XRD patterns of pure $BaTiO_3$ and Y-doped $BaTiO_3$ particles with different doping degree. It is found that the pure $BaTiO_3$

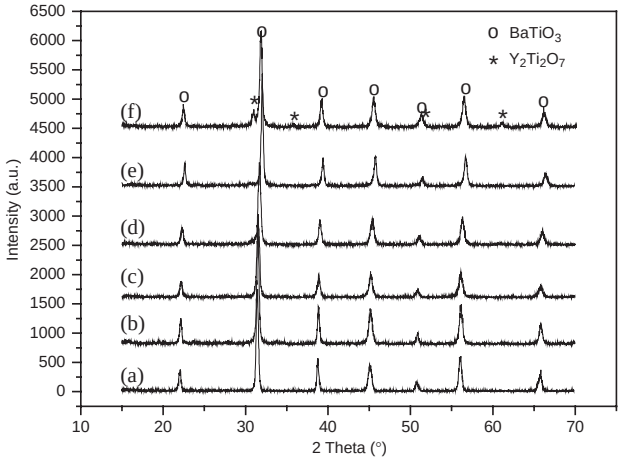

Fig. 4. XRD patterns of calcined powder with different Y-doping degree: (a) 0 mol%, (b) 1.8 mol%, (c) 4.4 mol%, (d) 8.9 mol%, (e) 13.8 mol%, and (f) 17.6 mol%.

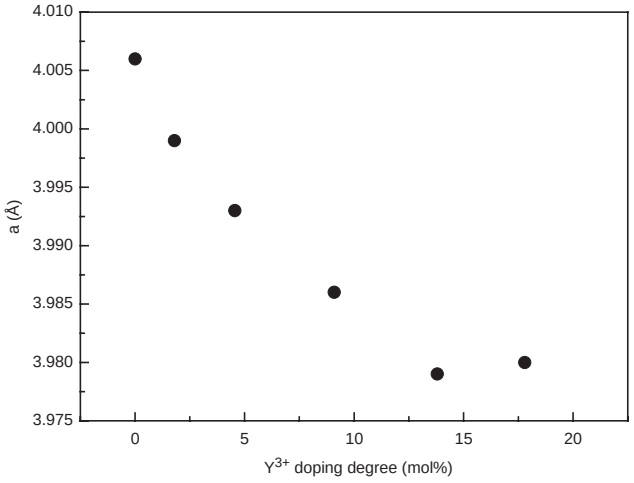

Fig. 5. Dependence of lattice parameter of Y-doped $BaTiO_3$ on Y^{3+} doping degree.

and doped $BaTiO_3$ all possess pure cubic phase since no split peaks are observed. This merits making a comparison about the properties of $BaTiO_3$ before and after doping. Furthermore, no other phase is found when doping degree is suitable. However, it is found that the peaks of doped $BaTiO_3$ shift towards a larger diffraction angle and the lattice parameters decrease with Y-doping degree (Fig. 5 is the change curve of lattice parameters with Y-doping degree.). These mean that small radius Y ions substitute for Ba site rather than Ti site, which may also be the reason of high-doping degree [49]. However, the values of lattice parameters do not change when the Y-doping degree exceeds 13.8 mol%, and some peaks due to $Y_2Ti_2O_7$ phase appear. This indicates that more Y ions fail to substitute for Ba when the doping degree is higher.

Fig. 6a shows the XPS survey spectrum of the typical 13.8 mol% Y-doped $BaTiO_3$ after calcination. The XPS peaks show that the particles contain only Ti, Ba, O, and Y and a trace amount of carbon. No other element is detected. The binding energies of Ti2p3, Ba3d5, O1s, and Y3d5 are 457.8, 779.1, 529.1, and 156.7 eV, respectively. In particular, the high-resolution XPS spectra of Y3d, Ba3d and Ti2p region show that the Y element corresponds to Y^{3+} (see the inset in Fig. 6a), Ba element corresponds to Ba^{2+}, and Ti element corresponds to Ti^{4+}. No Ti^{3+} is detected according to the Ti2p spectra (see Fig. 6b). Thus, the solid solution may be of the form $(Ba(II)_{1-x},Y(III)_x)Ti(IV)O_{3-x/2}$. Combining XPS with XRD, it is concluded that Y^{3+} substitutes for Ba^{2+}, which will often induce lattice-distorting defects and electric nonequilibrium [49–51]. The atom ratio of Y/Ba on the surface of the doped $BaTiO_3$ particles is determined from the ratio of peak areas corrected with the empirical sensitivity factors. The atomic ratio of Y/Ba is 0.097:1 in 8.9 mol% Y-doped $BaTiO_3$, which is in good agreement with the result of ICP. The atomic ratio of Y/Ba is 0.184:1 in 13.8 mol% Y-doped $BaTiO_3$ sample, which is slightly higher than the result of ICP measurement. However, the atomic ratio of Y/Ba is 0.308:1 in 17.6 mol% doped $BaTiO_3$ sample, which is significantly higher than the result of ICP measurement. This indicates more Y elements separate and exist on the surface of $BaTiO_3$ with $Y_2Ti_2O_7$ phase when the doping degree is too high. The C element is ascribed to the residual carbon from the adventitious hydrocarbon that is often observed in other samples.

3.2. Electrorheological properties

Figs. 7 and 8 show the flow curves of shear stress-shear rate for the pure $BaTiO_3$ and typical 13.8 mol% Y-doped $BaTiO_3$ suspensions at a volume fraction of 18%. In the absence of electric field, the flow curves of two suspensions are not in accordance with the flow curve of conventional dilute suspension that often shows a Newtonian fluid behavior. A shear-thin phenomena is found in two suspensions. This is attributed to the observed aggregation of $BaTiO_3$ particles due to their high dielectric constant [52]. In the presence of an electric field, the ER effect of pure $BaTiO_3$ suspension is very weak and its ER response does not show an obvious Bingham behavior. But the ER response of doped $BaTiO_3$ suspensions exhibit an obvious Bingham behavior, which represents typical ER effect (see Fig. 8). Furthermore, the electric field-enhanced shear stress, $\Delta\tau$, which was defined by relation $\Delta\tau = \tau_E - \tau_0$ (where τ_E is the shear stress at a shear rate $\dot{\gamma} = 10.51\ s^{-1}$ under electric field and τ_0 is the shear stress at a shear rate $\dot{\gamma} = 10.51\ s^{-1}$ under zero electric field) is over 0.6 kPa at 3 kV/mm for typical 13.8 mol% Y-doped $BaTiO_3$

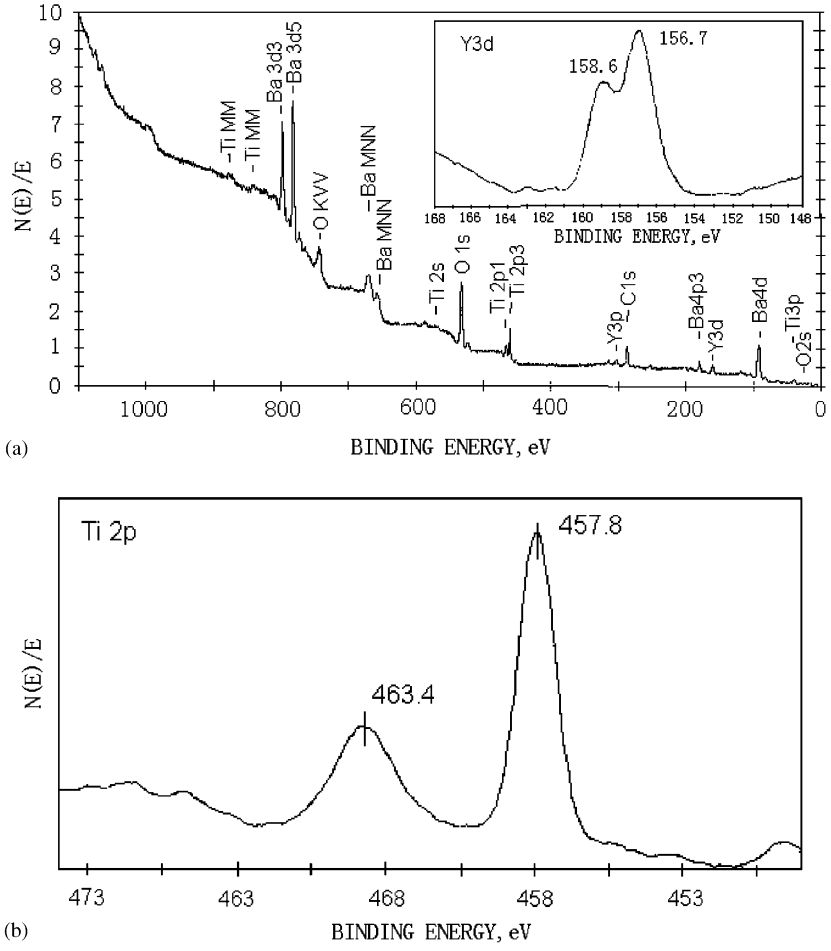

Fig. 6. (a) XPS survey spectrum of calcined 13.8 mol% Y-doped $BaTiO_3$ particles. An Y3d XPS spectrum is shown in inset. (b) Ti2p XPS spectra of calcined 13.8 mol% Y-doped $BaTiO_3$ particles.

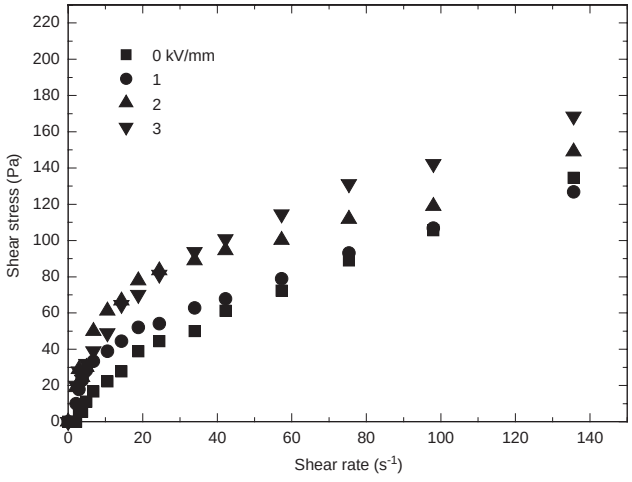

Fig. 7. Flow curve of shear stress of pure $BaTiO_3$ suspension as a function of shear rate at different dc electric field strengths (particle volume fraction = 18%, $T = 30°C$).

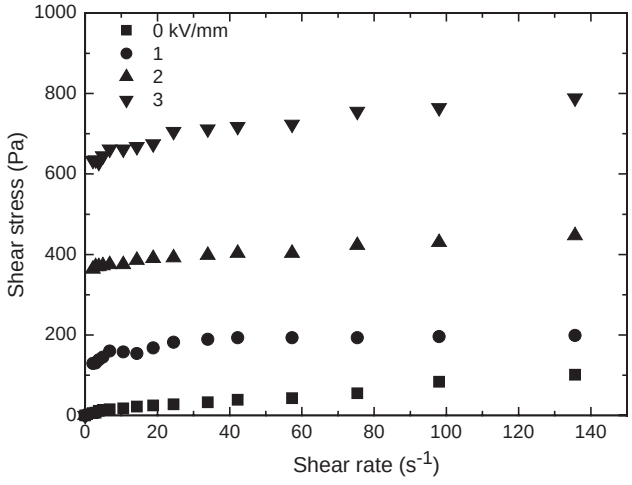

Fig. 8. Flow curve of shear stress of typical 13.8 mol% Y-doped $BaTiO_3$ suspension as a function of shear rate at different dc electric field strengths (particle volume fraction = 18%, $T = 30°C$).

suspension, which is ten times that of pure $BaTiO_3$. The corresponding current density is limited to 1.0 $\mu A/cm^2$. Because electric field-enhanced stress can clearly reflect the magnitude of ER effect [29]. This indicates that the doping indeed enhances ER activity of $BaTiO_3$ under dc electric field.

Fig. 9 shows the electric field-enhanced shear stress as a function of electric field between the pure $BaTiO_3$ and doped $BaTiO_3$ suspensions. It can be clearly found that $\Delta\tau$ of doped $BaTiO_3$ suspension is much higher than that of pure $BaTiO_3$ suspension. The optimal doping degree for large ER enhancement is in the range 9–15 mol% (see Fig. 10) and the ER effect declines when doping degree is too high. Furthermore, it should be noted that the other $Y_2Ti_2O_7$ phases also appear in sample with higher doping degree according to XRD patterns. The appearance of these second phases may be an important factor that results in the decrease of ER properties. In order to verify the effect of doping on ER activity, we prepare pure Y_2O_3 powers from $Y(NO_3)_3$ and investigate ER properties of the pure Y_2O_3/silicone oil suspension and the suspensions composed of cubic

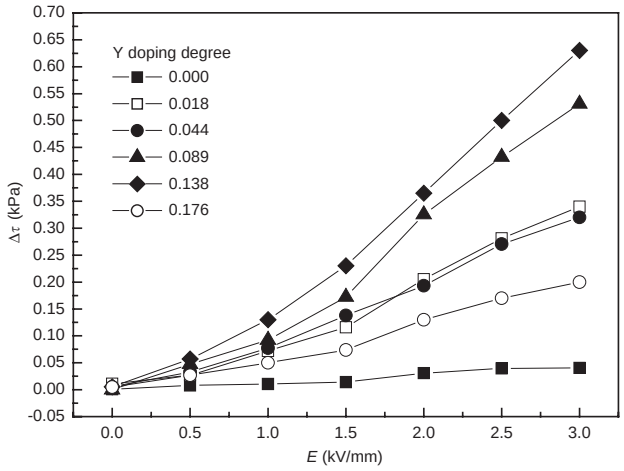

Fig. 9. Electric field-enhanced shear stress of pure $BaTiO_3$ suspension and Y-doped $BaTiO_3$ suspension as a function of dc electrical field strength (particle volume fraction = 18%, $T = 30°C$, $\dot{\gamma} = 10.51\ s^{-1}$).

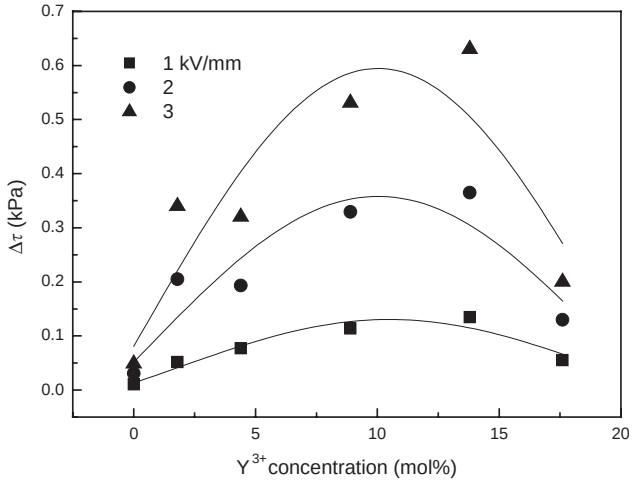

Fig. 10. Dependence of electric field-enhanced shear stress of Y-doped $BaTiO_3$ suspension on Y^{3+} doping degree at different dc electrical fields (particle volume fraction = 18%, $T = 30°C$, $\dot{\gamma} = 10.51\ s^{-1}$).

$BaTiO_3$ and Y_2O_3. As we expected, $\Delta\tau$ is very low, about 80 Pa (3 kV/mm), in the 18 vol% pure Y_2O_3 suspension. $\Delta\tau$ of all the ER suspensions made of a simple mixture of $BaTiO_3$ and Y_2O_3 with different Y_2O_3 content are even lower than 80 Pa at 3 kV/mm. This striking difference in ER activity between doped $BaTiO_3$ and the simple mixture clearly indicates that suitable Y-doping into $BaTiO_3$ is the key to enhancement of ER activity of $BaTiO_3$ under dc electric field.

3.3. Fibrillation structure and electrical properties

In order to preliminarily understand this ER material, we observed the static fibrillation structure of ER suspension under a dc electric field and measured its electrical properties. Part a and b of Fig. 11 show the fibrillation structure of pure $BaTiO_3$ and doped $BaTiO_3$ suspensions, respectively. With no electric field, the particles of pure $BaTiO_3$ (Fig. 11a) and doped $BaTiO_3$ (Fig. 11b) suspensions are freely dispersed in silicone oil and some aggregations of $BaTiO_3$ particles are also found. When 2 kV/mm electric field is applied, it is found that the pure $BaTiO_3$ particles do not quickly form a chain structure but exhibit obvious electrophoretic effect. Only some thin chains are found in this pure $BaTiO_3$ suspension when 2 kV/mm electric field is applied for 30 s, but there are still many electrophoretic particles (see Fig. 11a). In particular, the continuous application of this dc electric field is found to result in the accumulation of $BaTiO_3$ particles on the positive electrode. Thus, it can be deduced that the electrophoretic effects, which disrupt the formation of chains structure, may be the main factor resulting in low-yield stress of $BaTiO_3$ suspension under dc electrical field. On the contrary, the particles in Y-doped $BaTiO_3$ suspension can quickly form chain structures as soon as 2 kV/mm dc electric field is applied. No electrophoretic particles are found. This infers that the Y-doping effectively neutralizes the charges of $BaTiO_3$ particles, which cause electrophoretic effects. Furthermore, we also note that the chains in Y-doped $BaTiO_3$ suspension occur to congregate and become thicker as long as the electric field is applied. Fig. 11b shows the static structures images of this doped $BaTiO_3$ suspension when 2 kV/mm dc electric field is applied for 30 s. Obviously, these thicker chain clusters will merit large-yield stress. Therefore, comparing the rheological properties with the static structure evolvement images, it can be concluded that Y-doping indeed enhances ER activity of $BaTiO_3$ under dc electric field.

According to wide ER investigations [1,12,29,37,39,40], the dielectric and conduction properties of ER materials are considered to be important to the ER effect. In particular, the interaction force between particles is proportional to the factors $2\varepsilon_f\varepsilon_0(\beta E)^2$, where ε_f is the dielectric constant of oil phase, ε_0 is the

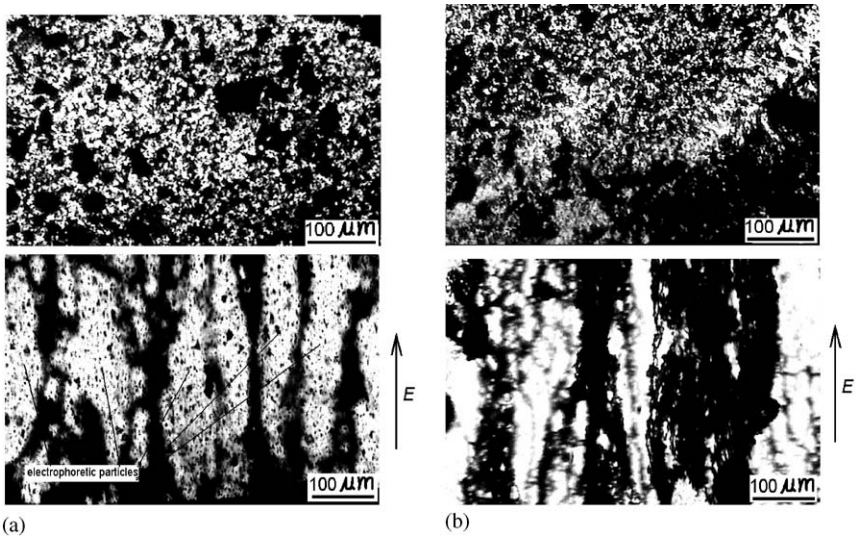

Fig. 11. Photographs of structure without electric field and after application of 2 kV/mm dc electric field for 30 s (a) pure $BaTiO_3$ and (b) 13.8 mol% Y-doped $BaTiO_3$ suspensions (particle volume fraction = 5%, $T = 30°C$).

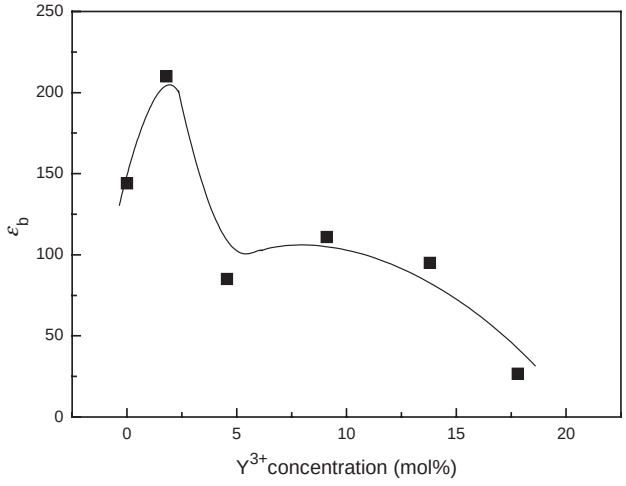

Fig. 12. Dependence of dielectric constant of Y-doped $BaTiO_3$ bulk on Y^{3+} doping degree at 10^3 Hz.

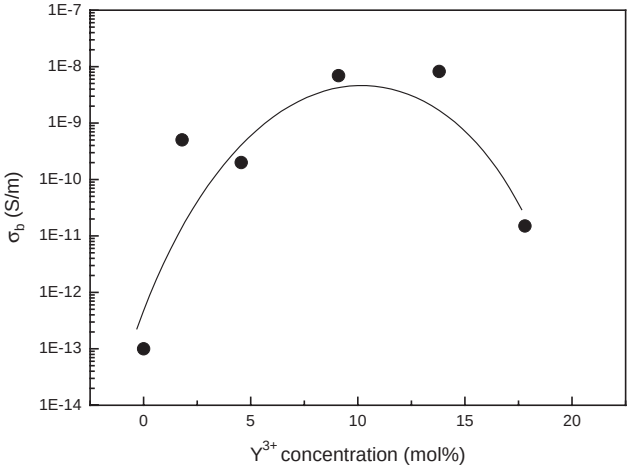

Fig. 13. Dependence of dc conductivity of Y-doped $BaTiO_3$ bulk on Y^{3+} doping degree.

dielectric constant of vacuum, E is the applied electric field strength, and β is the mismatch factor of dielectric and conduction parameters between particles and oil phase. Under dc or low frequency ac electric field, the large conductivity mismatch, $\beta = (\sigma_p - \sigma_f)/(\sigma_p + 2\sigma_f)$ (where σ_p is the conductivity of dispersed particles and σ_f is the conductivity of the oil phase), between particles and oil phase is considered to be more important to the ER effect than dielectric constant mismatch, $\beta = (\varepsilon_p - \varepsilon_f)/(\varepsilon_p + 2\varepsilon_f)$ (where ε_p is the conductivity of dispersed particles and ε_f is the conductivity of oil phase), between particles and oil phase [53–55]. Figs. 12 and 13 show the typical dielectric constant of doped $BaTiO_3$ with doping degree at 10^3 Hz and dc conductivity at room temperature, respectively. It is found that the dielectric constant of pure $BaTiO_3$ is relative high but its conductivity is very low. According to the suggested ER mechanics above or other investigations about $BaTiO_3$ [33–38], the very low conductivity of pure $BaTiO_3$ may be an important factor to low ER activity under dc electric field although its dielectric constant is high. Here, doping rare earth ions initially increase dielectric constant and further doping decreases the dielectric constant to some extent, but the conductivity of $BaTiO_3$ is obviously improved due to Y-doping and a higher conductivity can be obtained when the doping degree is in a suitable range of 9–15 mol%. Fig. 14 gives a link between the electric field-enhanced shear stress and conductivity. It can be found that the ER effect of $BaTiO_3$ increases with the enhancement of conductivity. When the doping degree is higher, the conductivity is found to obviously decrease and stress also decreases,

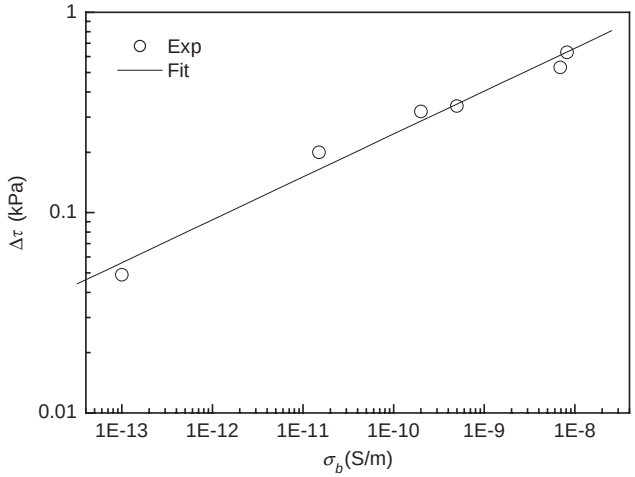

Fig. 14. Relationship between electric field-enhanced shear stress and dc conductivity of Y-doped $BaTiO_3$ bulk.

which may be attributed to the obvious phase separation of $Y_2Ti_2O_7$ from $BaTiO_3$, according to XRD patterns. However, the ER effect does not show a regular change with dielectric constant. Furthermore, because the synthesized $BaTiO_3$ and doped $BaTiO_3$ are cubic phases, no ferroelectric effect influences the electric and electrorheological properties here. Therefore, the contribution from improvement in conductivity due to rare earth ions doping may be a very important factor in the enhancement of ER activity of $BaTiO_3$.

4. Conclusion

In this study, we choose cubic $BaTiO_3$ and first achieve its ER enhancement under dc electric field by modifying its intrinsic structure with doping rare earth Y ions, which is synthesized by means of sol–gel technique. Structure characterizations show that Y^{3+} substitutes for Ba^{2+}, which causes lattice-distorting defects. The pure $BaTiO_3$ and Y-doped $BaTiO_3$ particles are used as ER suspension by dispersing them in silicone oil. It is found that pure cubic $BaTiO_3$ is very weak in ER activity and even suffered from electrophoretic effects under dc electric field, while Y-doped $BaTiO_3$ shows a notable ER activity and the Y-doping degree is demonstrated to have an influence on the ER activity. Based on the chain structure and electrical measurements, the increase of conductivity of $BaTiO_3$ due to Y-doping may be responsible for the enhancement of ER activity. This enhancement in ER activity of cubic $BaTiO_3$ under dc electric field by doping rare earth Y ions is helpful to further understand low ER activity of the perovskite-based ER materials.

Acknowledgments

We are grateful for the help from Prof. Z.Q. Guo for the XRD, Associate Prof. J. Lu and Dr. H.L. Guo for FT-IR, and DSC-TG, Dr. X.Y. Li for XPS, Associate Prof. F.X. Dong for ICP, and X.Y. Yu for SEM measurements. Financial support for this research has come from the National Natural Science Foundation of China for distinguished Young Scholars program (No.50025207) and the National Natural Science Foundation of China (No. 50272054).

References

[1] H. Block, J.P. Kelly, J. Phys. D: Appl. Phys. 21 (1988) 1661.
[2] T.C. Halsey, Science 258 (1992) 761.
[3] M. Parthasarathy, D.J. Klingenberg, Mater. Sci. Eng. R 17 (1996) 57.
[4] S.P. Couter, K.D. Weiss, J.D. Carlson, J. Intel. Mater. Syst. Struct. 4 (1993) 248.
[5] T. Hao, Adv. Mater. 13 (2001) 1847.
[6] J.J. Fan, X.P. Zhao, X.M. Gao, C.N. Cao, J. Phys. D: Appl. Phys. 35 (2002) 88.
[7] X.P. Zhao, Q. Zhao, X.M. Gao, J. Appl. Phys. 93 (2003) 4309.
[8] (a) H.X. Guo, X.P. Zhao, G.H. Ning, G.Q. Liu, Langmuir 19 (2003) 4884;
(b) T.Y. Gong, D.T. Wu, D.W.M. Marr, Langmuir 19 (2003) 5967.
[9] F.Q. Yang, J. Colloid Interface Sci. 192 (1997) 162.
[10] X. Tang, X. Zhang, R. Tao, J. Appl. Phys. 87 (2000) 2634.
[11] K.C. Lau, L. Shi, W.Y. Tam, P. Sheng, Phys. Rev. E 67 (2003) 52502.
[12] H. Block, J.P. Kelly, A. Qin, T. Wastson, Langmuir 6 (1990) 6.
[13] I.S. Sim, J.W. Kim, H.J. Choi, C.A. Kim, M.S. Jhon, Chem. Mater. 13 (2001) 1243.
[14] F.E. Filisko, L.H. Radzilowski, J. Rheol. 34 (1990) 539.
[15] R. Bloodworth, in: R. Tao, G.D. Roy (Eds.), Proceeding of the Fourth International Conference on ER Fluids-Mechanisms, Properties, Technology and Applications, World Scientific, Singapore, 1994, p. 67.
[16] R. Sakurai, H. See, T. Saito, J. Rheol. 40 (1996) 395.
[17] W.Y. Tam, G.H. Yi, W. Wen, H. Ma, M.M.T. Loy, P. Sheng, Phys. Rev. Lett. 78 (1997) 2987.
[18] L.Q. Xiang, X.P. Zhao, J. Mater. Chem. 13 (2003) 1529.
[19] J.W. Kim, M.H. Noh, H.J. Choi, D.C. Lee, M.S. Jhon, Polymer 41 (2000) 1229.
[20] X.P. Zhao, X. Duan, J. Colloid Interface Sci. 251 (2002) 376.
[21] Y.T. Lim, J.H. Park, O.O. Park, J. Colloid Interface Sci. 245 (2002) 198.
[22] B.X. Wang, X.P. Zhao, J. Mater. Chem. 12 (2002) 1863.
[23] J. Lu, X.P. Zhao, J. Mater. Chem. 12 (2002) 2603.
[24] Y. Otsubo, K. Watanabe, J. Soc. Rheol. Jpn. 18 (1990) 111.
[25] T. Garino, D. Adolf, B. Hance, in: R. Tao (Ed.), Proceeding of the Third International Conference on ER Fluids—Mechanisms, Properties, Technology and Applications, World Scientific, Singapore, 1992, p. 67.
[26] C.F. Zukoski, Annu. Rev. Mater. Sci. 23 (1993) 45.
[27] D.V. Miller, C.A. Randall, A.S. Bhalla, R.E. Newnham, J.H. Adair, Ferroelectr. Lett. Sect. 15 (1993) 114.
[28] J.M. Ginder, S.L. Cecio, J. Rheol. 35 (1995) 211.
[29] H. Block, P. Rattay, in: K.O. Havelka, F.E. Filisko (Eds.), Progress in Electrorheology, Plenum Press, New York, 1995, p. 19.

[30] P.J. Rankin, D.J. Klingenberg, J. Rheol. 42 (1998) 639.
[31] W.J. Wen, W.Y. Tam, P. Sheng, J. Mater. Res. 13 (1998) 2783.
[32] Y.C. Lan, S.Q. Men, X.P. Zhao, K.Q. Lu, Appl. Phys. Lett. 72 (1998) 653.
[33] C. Bossiy, et al., Int. J. Mod. Phys. B 13 (14–16) (1999) 1775.
[34] H. Böse, A. Trendler, in: R. Tao (Ed.), Proceeding of the Seventh International Conference on Electrorheological Fluids and Magnetorheological Suspensions, World Scientific, Singapore, 2000, p. 44.
[35] T. Misono, T. Yamaguchi, K. Negita, J. Mol. Liq. 90 (2001) 333.
[36] T. Hao, Appl. Phys. Lett. 70 (1997) 1956.
[37] T. Hao, A. Kawai, F. Ikazaki, Langmuir 14 (1998) 1256.
[38] A. Kawai, E. Nakamura, S. Yano, Ferroelectrics 255 (2001) 47.
[39] F. Ikzaki, A. Kawai, K. Uchida, T. Kawakami, K. Edmura, K. Sakurai, H. Anzai, Y. Asako, J. Phys. D: Appl. Phys. 31 (1998) 336.
[40] A. Kawai, Y. Ide, A. Inoue, F. Ikzaki, J. Chem. Phys. 109 (1998) 4587.
[41] J.B. Yin, X.P. Zhao, J. Phys. D: Appl. Phys. 34 (2001) 2063.
[42] X.P. Zhao, J.B. Yin, Chem. Mater. 14 (2002) 2258.
[43] J.B. Yin, X.P. Zhao, Chem. Mater. 14 (2002) 4633.
[44] J.B. Yin, X.P. Zhao, J. Mater. Chem. 13 (2003) 689.
[45] J.B. Yin, X.P. Zhao, Chem. Mater. 16 (2004) 321.
[46] X.P. Zhao, J.B. Yin, Chin. Pat. 2000, CN00113930.4
[47] J. Nowotny, M. Rekas, Key Eng. Mater. 66–67 (1992) 1.
[48] M.H. Lin, H.Y. Lu, Mater. Sci. Eng. A 3 (2001) 1205.
[49] K. Kowalski, M. Ijjaali, T. Bakb, B. Dupre, J. Nowotnyb, M. Rekas, C.C. Sorrell, J. Phys. Chem. Solids 62 (2001) 543.
[50] F.D. Morrison, D.C. Sinclair, A.R. West, J. Appl. Phys. 86 (1999) 6355.
[51] Y. Tsur, T.D. Dunbar, C.A. Randall, J. Electroceram. 7 (2001) 25.
[52] D. Khastgir, K. Adachi, Polymer 41 (2000) 6403.
[53] L.C. Davis, J. Appl. Phys. 72 (1992) 1334.
[54] P. Atten, J.-N. Foulc, N. Felici, Int. J. Mod. Phys. B 8 (1994) 2731.
[55] X. Tang, C. Wu, H. Conrad, J. Rheol. 39 (1995) 1059.